Probing the Deuteron at Very Large Internal Momenta

C. Yero,[1,15,*] D. Abrams,[2] Z. Ahmed,[3] A. Ahmidouch,[4] B. Aljawrneh,[4] S. Alsalmi,[5] R. Ambrose,[3] W. Armstrong,[6] A. Asaturyan,[7] K. Assumin-Gyimah,[8] C. Ayerbe Gayoso,[9] A. Bandari,[9] J. Bane,[10] S. Basnet,[3] V. V. Berdnikov,[11] J. Bericic,[15] H. Bhatt,[8] D. Bhetuwal,[8] D. Biswas,[12] W. U. Boeglin,[1] P. Bosted,[9] E. Brash,[13] M. H. S. Bukhari,[14] H. Chen,[2] J. P. Chen,[15] M. Chen,[2] M. E. Christy,[12] S. Covrig,[15] K. Craycraft,[10] S. Danagoulian,[4] D. Day,[2] M. Diefenthaler,[15] M. Dlamini,[17] J. Dunne,[8] B. Duran,[16] D. Dutta,[8] R. Ent,[15] R. Evans,[3] H. Fenker,[15] N. Fomin,[10] E. Fuchey,[18] D. Gaskell,[15] T. N. Gautam,[12] F. A. Gonzalez,[19] J. O. Hansen,[15] F. Hauenstein,[20] A. V. Hernandez,[11] T. Horn,[11] G. M. Huber,[3] M. K. Jones,[15] S. Joosten,[6] M. L. Kabir,[8] A. Karki,[8] C. E. Keppel,[15] A. Khanal,[1] P. King,[17] E. Kinney,[21] N. Lashley-Colthirst,[12] S. Li,[22] W. B. Li,[9] A. H. Liyanage,[12] D. J. Mack,[15] S. P. Malace,[15] J. Matter,[2] D. Meekins,[15] R. Michaels,[15] A. Mkrtchyan,[7] H. Mkrtchyan,[7] S. J. Nazeer,[12] S. Nanda,[8] G. Niculescu,[23] M. Niculescu,[23] D. Nguyen,[2] N. Nuruzzaman,[24] B. Pandey,[12] S. Park,[19] C. F. Perdrisat,[9] E. Pooser,[15] M. Rehfuss,[16] J. Reinhold,[1] B. Sawatzky,[15] G. R. Smith,[15] A. Sun,[25] H. Szumila-Vance,[15] V. Tadevosyan,[7] S. A. Wood,[15] and J. Zhang[19]

(Hall C Collaboration)

[1]*Florida International University, University Park, Florida 33199, USA*
[2]*University of Virginia, Charlottesville, Virginia 22903, USA*
[3]*University of Regina, Regina, Saskatchewan S4S 0A2, Canada*
[4]*North Carolina Agricultural and Technical State University, Greensboro, North Carolina 27411, USA*
[5]*Kent State University, Kent, Ohio 44240, USA*
[6]*Argonne National Laboratory, Lemont, Illinois 60439, USA*
[7]*A.I. Alikhanyan National Science Laboratory (Yerevan Physics Institute), 2 Alikhanian Brothers Street, 0036, Yerevan, Armenia*
[8]*Mississippi State University, Mississippi State, Mississippi 39762, USA*
[9]*College of William & Mary, Williamsburg, Virginia 23185, USA*
[10]*University of Tennessee, Knoxville, Tennessee 37996, USA*
[11]*Catholic University of America, Washington, D.C. 20064, USA*
[12]*Hampton University, Hampton, Virginia 23669, USA*
[13]*Christopher Newport University, Newport News, Virginia 23606, USA*
[14]*Jazan University, Jazan 45142, Saudi Arabia*
[15]*Thomas Jefferson National Accelerator Facility, Newport News, Virginia 23606, USA*
[16]*Temple University, Philadelphia, Pennsylvania 19122, USA*
[17]*Ohio University, Athens, Ohio 45701, USA*
[18]*University of Connecticut, Storrs, Connecticut 06269, USA*
[19]*Stony Brook University, Stony Brook, New York 11794, USA*
[20]*Old Dominion University, Norfolk, Virginia 23529, USA*
[21]*University of Colorado Boulder, Boulder, Colorado 80309, USA*
[22]*University of New Hampshire, Durham, New Hampshire 03824, USA*
[23]*James Madison University, Harrisonburg, Virginia 22807, USA*
[24]*Rutgers University, New Brunswick, New Jersey 08854, USA*
[25]*Carnegie Mellon University, Pittsburgh, Pennsylvania 15213, USA*

(Received 19 August 2020; revised 27 October 2020; accepted 2 December 2020; published 29 December 2020)

We measure $^2\mathrm{H}(e,e'p)n$ cross sections at 4-momentum transfers of $Q^2 = 4.5 \pm 0.5$ $(\mathrm{GeV}/c)^2$ over a range of neutron recoil momenta p_r, reaching up to $\sim$1.0 GeV/c. We obtain data at fixed neutron recoil angles $\theta_{nq} = 35°$, 45°, and 75° with respect to the 3-momentum transfer $\vec{q}$. The new data agree well with previous data, which reached $p_r \sim 500$ MeV/c. At $\theta_{nq} = 35°$ and 45°, final state interactions, meson exchange currents, and isobar currents are suppressed and the plane wave impulse approximation provides the dominant cross section contribution. We compare the new data to recent theoretical calculations, where we observe a significant discrepancy for recoil momenta $p_r > 700$ MeV/c.

DOI: 10.1103/PhysRevLett.125.262501

The deuteron is the only bound two-nucleon system and serves as an ideal framework to study the strong nuclear force at the sub-Fermi distance scale, a region that is currently practically unexplored and not well understood. Understanding the high-momentum structure of the proton-neutron (pn) system is highly important for nuclear physics due to the observed dominance of short-range correlations in nuclei at nucleon momenta above the Fermi momentum. This dominance has been well established by a series of recent experiments carried out at Jefferson Lab (JLab) [1–4] and Brookhaven National Laboratory [5]. In these experiments, missing momenta up to $\sim$1 GeV/c have been probed and missing momentum distributions have been compared to the high-momentum part of theoretical deuteron momentum distributions. Missing momenta up to $\sim$1 GeV/c have also been probed in a ^{3}He$(e,e'p)$ experiment [6,7] but at a relatively low-momentum transfer of 1.5 $(\mathrm{GeV}/c)^2$ and at a kinematic region (Bjorken $x_B \sim 1$), where the cross section is dominated by final state interactions. Because of final state interaction (FSI) effects, the measurement of a certain missing momentum does not yet guarantee that the initial bound nucleon with the same momentum is being measured.

The most direct way to study the short-range structure of the deuteron wave function is via the exclusive deuteron electrodisintegration reaction at internal momenta $p_r > 300$ MeV/c. For ^{2}H$(e,e'p)n$, within the plane wave impulse approximation (PWIA), the virtual photon couples to the bound proton, which is subsequently ejected from the nucleus without further interaction with the recoiling system (neutron). The neutron carries a recoil momentum p_r equal in magnitude but opposite in direction to the initial state proton, $\vec{p}_r \sim -\vec{p}_{i,p}$, thus providing information on the momentum of the bound nucleon and its momentum distribution.

In addition to the PWIA picture, the ejected nucleon undergoes FSIs with the recoiling nucleon. Other contributing processes are the photon coupling to the exchanged mesons in the pn system, generating meson exchange currents (MECs), or the photon exciting the bound nucleon into the resonating state (mainly Δ isobar) with subsequent $\Delta N \to NN$ rescattering, referred to as isobar currents (ICs). FSIs, MECs, and ICs can significantly alter the recoiling neutron momentum, thereby obscuring the original momentum of the bound nucleon and reducing the possibility of directly probing the deuteron momentum distribution.

Theoretically, MECs and ICs are expected to be suppressed at $Q^2 > 1$ $(\mathrm{GeV}/c)^2$ and Bjorken $x_B \equiv Q^2/2M_p\omega > 1$, where M_p and ω are the proton mass and photon energy transfer, respectively [8]. The suppression of MECs can be understood from the fact that the estimated MEC scattering amplitude is proportional to $(1+Q^2/m^2_{\mathrm{meson}})^{-2}(1+Q^2/\Lambda^2)^{-2}$, where $m_{\mathrm{meson}} \approx 0.71$ GeV/c^2 and $\Lambda^2 \sim 0.8$–1 $(\mathrm{GeV}/c)^2$ [9]; this results in an additional $1/Q^4$ suppression as compared to the quasielastic contribution. Note that other meson exchange contributions that take place before the virtual photon interaction are included in the definition of the ground state wave function of the deuteron. ICs can be suppressed kinematically by selecting $x_B > 1$, where one probes the lower energy (ω) part of the deuteron quasielastic peak, which is maximally away from the inelastic resonance electroproduction threshold. Previous deuteron electrodisintegration experiments performed at lower Q^2 $[Q^2 < 1$ $(\mathrm{GeV}/c)^2]$ (see Sec. 5 of Ref. [8]) have helped quantify the contributions from FSIs, MECs, and ICs to the ^{2}H$(e,e'p)n$ cross sections and to determine the kinematics at which they are either suppressed (MECs and ICs) or under control (FSIs).

At large Q^2, FSIs can be described by the generalized eikonal approximation (GEA) [8–10], which predicts a strong dependence of FSIs on neutron recoil angles θ_{nq} (relative angles between recoil momenta $\vec{p}_r$ and 3-momentum transfers $\vec{q}$). GEA predicts FSIs to be maximal for $\theta_{nq} \sim 70°$. This strong angular dependence has been found to lead to the cancellation of FSIs at neutron recoil angles around $\theta_{nq} \sim 40°$ and $\theta_{nq} \sim 120°$. Because at $\theta_{nq} \sim 120°$ ($x_B < 1$) ICs are not negligible, the $x_B > 1$ ($\theta_{nq} \sim 40°$) kinematics are the preferred choice to suppress ICs as well as FSIs.

The first ^{2}H$(e,e'p)n$ experiments at high Q^2 $[> 1$ $(\mathrm{GeV}/c)^2]$ were carried out at JLab in Halls A [11] and B [12]. Both experiments determined that the cross sections for fixed recoil momenta indeed exhibited a strong angular dependence with θ_{nq}, peaking at $\theta_{nq} \sim 70°$ in agreement with GEA [9,10] calculations. In Hall B, the Continuous Electron Beam Accelerator Facility Large Acceptance Spectrometer measured angular distributions for a range of Q^2 values as well as momentum distributions. However, statistical limitations made it necessary to integrate over a wide angular range to determine momentum distributions, which are therefore dominated by FSIs, MECs, and ICs for p_r above $\sim$300 MeV/c.

In the Hall A experiment [11], the pair of high-resolution spectrometers made it possible to measure the p_r dependence of the cross section for fixed θ_{nq} reaching recoil momenta up to $p_r = 550$ MeV/c at $Q^2 = 3.5 \pm 0.25$ $(\mathrm{GeV}/c)^2$. For the first time, very different momentum distributions were found for $\theta_{nq} = 35 \pm 5°$ and $45 \pm 5°$ compared to $\theta_{nq} = 75 \pm 5°$. Theoretical models attributed this difference to the suppression of FSIs at the smaller angles ($\theta_{nq} = 35$, $45°$) compared to FSIs dominance at $\theta_{nq} = 75°$ [11].

The experiment presented in this Letter takes advantage of the kinematic window previously found in the Hall A experiment [11] and extends the ^{2}H$(e,e'p)n$ cross section measurements to $Q^2 = 4.5 \pm 0.5$ $(\mathrm{GeV}/c)^2$ and recoil momenta up to $p_r \sim 1$ GeV/c, which is almost double the maximum recoil momentum measured in Hall A [11].

Measurements at such large Q^2 and high p_r required scattered electrons to be detected at ~8.5 GeV/c, which was only made possible with the newly commissioned Hall C super-high-momentum spectrometer (SHMS). At the selected kinematic settings with $35° \leq \theta_{nq} \leq 45°$, MECs and ICs are suppressed and FSIs are under control, giving access to high-momentum components of the deuteron wave function.

A 10.6 GeV electron beam was incident on a 10-cm-long liquid deuterium target. The scattered electron and knocked-out proton were detected in coincidence by the new SHMS and the existing high-momentum spectrometer (HMS), respectively. The beam currents delivered by the accelerator ranged between 45 and 60 μA and the beam was rastered over a 2×2 mm^2 area to reduce the effects of localized boiling on the cryogenic targets.

Both Hall C spectrometers have similar standard detector packages [13], each with four scintillator planes used for triggering, a pair of drift chambers used for tracking, and a calorimeter and gas Čerenkov used for electron identification. For each spectrometer, a logic signal was created from the coincidence of hits in at least three of the four scintillator planes. The event trigger was the coincidence of these two signals.

We measured three central recoil momentum settings: $p_r = 80$, 580 and 750 MeV/c. At each of these settings, the electron arm (SHMS) was fixed and the proton arm (HMS) was rotated from smaller to larger angles corresponding to the lower and higher recoil momentum settings, respectively. At these kinematic settings, the 3-momentum transfer covered a range of $2.4 \lesssim |\vec{q}| \lesssim 3.2$ GeV/c, which is more than twice the highest neutron recoil momentum measured in this experiment. As a result, most of the virtual photon momentum is transferred to the proton, which scatters at angles relative to $\vec{q}$ in the range $0.4° \lesssim \theta_{pq} \lesssim 21.4°$. At these forward angles and large momenta transferred to the proton, the process where the neutron is struck by the virtual photon is suppressed.

Hydrogen elastic $^1\mathrm{H}(e, e'p)$ data were also taken at kinematics close to the deuteron $p_r = 80$ MeV/c setting for cross-checks with the spectrometer acceptance model using the Hall C Monte Carlo simulation program, SIMC [14]. Additional $^1\mathrm{H}(e, e'p)$ data were also taken at three other kinematic settings that covered the SHMS momentum acceptance range for the deuteron and were used for spectrometer optics optimization, momentum calibration, and the determination of the spectrometer offsets and kinematic uncertainties [13].

Identical event selection criteria were used for the hydrogen and deuteron data. The criteria were determined by making standard cuts on the spectrometer momentum fraction (δ) to select a region for which the reconstruction optics are well known: a cut to restrict the HMS solid angle acceptance to events that passed directly through the collimator and not by rescattering from the collimator edges, a reconstructed binding energy cut (peak ~2.22 MeV for the deuteron) to select true $^2\mathrm{H}(e, e'p)n$ coincidences, a coincidence time cut to select true coincidence events, a particle identification cut on the SHMS calorimeter normalized total track energy to select electrons and not other sources of background (mostly pions), and a cut on the reconstructed HMS and SHMS reaction vertices to select events that originated from the same reaction vertex at the target (see Supplemental Material [15]).

The experimental data yield for both hydrogen and deuteron data were normalized by the total charge and corrected for various inefficiencies. For $^2\mathrm{H}(e, e'p)n$, the corrections were as follows [13]: tracking efficiencies (98.9% HMS, 96.4% SHMS), total live time (92.3%), proton loss inefficiency due to nuclear interactions in the HMS (4.7%), and target boiling inefficiency (4.2%). The values in parentheses were averaged over all recoil momentum settings.

For $^1\mathrm{H}(e, e'p)$, the corrected data yield was compared to SIMC calculations using Arrington's proton form factor (FF) parametrization [18] to check the spectrometer acceptance model. The ratio of data to simulation yield was determined to be $97.6 \pm 0.3\%$ (statistical uncertainty only).

The systematic uncertainties on the measured cross sections were determined from normalization and kinematic uncertainties in the beam energy and spectrometer angle and momentum settings. The individual contributions from normalization uncertainties for each setting were determined to be (on average) [13]: tracking efficiencies (0.40% HMS, 0.59% SHMS) and target boiling (0.38%), which were added in quadrature and determined to be about 0.81% per setting. This result was then added quadratically to the systematic uncertainties due to proton loss in HMS (0.49%), total live time (3.0%), total charge (2.0%), target wall contributions ($\leq 2.9\%$), and spectrometer acceptance (1.4%), which were the same for every setting, to define the overall normalization uncertainty ($\leq 5.3\%$).

The systematic uncertainties due to the systematic error on the absolute beam energy and spectrometer angle and momentum settings were determined point-to-point in (θ_{nq}, p_r) bins for each recoil momentum setting and added in quadrature for overlapping p_r bins. For $\theta_{nq} = 35°$, 45°, and 75° (presented in this Letter), the overall kinematic uncertainty varied below 6.5%. The total uncertainty was defined as the quadrature sum of the normalization ($\leq 5.3\%$), kinematic ($\leq 6.5\%$), and statistical (~20%–30% on average) uncertainties.

The data were radiatively corrected for each bin in (θ_{nq}, p_r) by multiplying the measured cross sections by the ratio of the calculated particle yield, excluding and including radiative effects. The SIMC simulation code was used for these calculations with the Deuteron Model by Laget including FSIs [19]. For each bin in (θ_{nq}, p_r), the averaged $^2\mathrm{H}(e, e'p)n$ kinematics was calculated and used in the bin-centering correction factor, defined as $f_{\mathrm{bc}} \equiv \sigma_{\mathrm{avg.kin}}/\bar{\sigma}$,

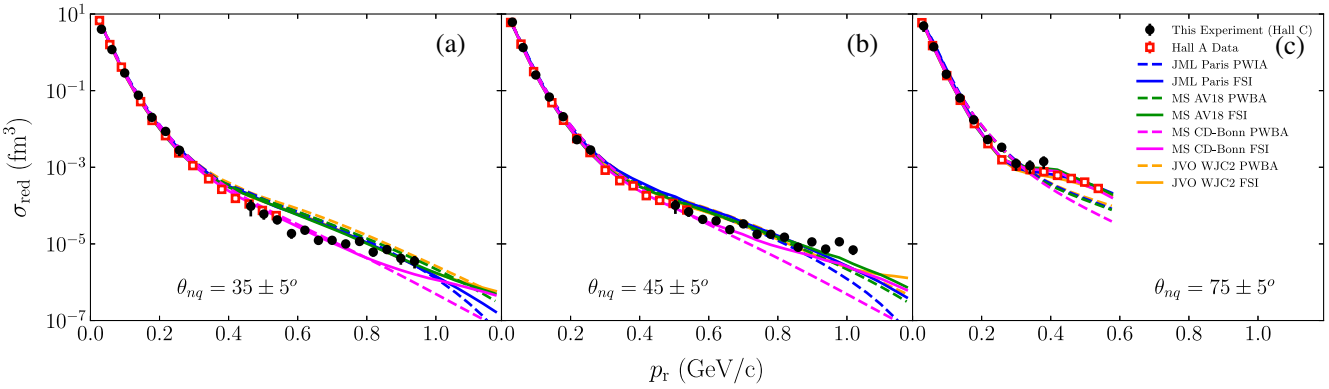

FIG. 1. The reduced cross sections $\sigma_{\rm red}(p_r)$ as a function of neutron recoil momentum p_r are shown in (a)–(c) for recoil angles $\theta_{nq} = 35°$, 45°, and 75°, respectively, with a bin width of ±5°. The data are compared to the previous Hall A experiment (red square) results [11], as well as the theoretical reduced cross sections using the Paris (blue), AV18 (green), CD-Bonn (magenta), and WJC2 (orange) NN potentials. The plane wave born approximation (PWBA) includes the PWIA and the process in which the virtual photon couples to the neutron and the proton emerges as a spectator without subsequent reinteractions (no FSIs).

where $\sigma_{\rm avg.kin}$ is the cross section calculated at the averaged kinematics and $\bar{\sigma}$ is the cross section averaged over the kinematic bin. The systematic uncertainties associated with the radiative and bin-centering corrections were investigated using the Laget PWIA and FSI models but negligible effects on the cross sections were found (see Supplemental Material [15]). The experimental and theoretical reduced cross sections were extracted and are defined as follows:

$$\sigma_{\rm red} \equiv \frac{\sigma_{\rm exp(th)}}{E_f p_f f_{\rm rec} \sigma_{\rm cc1}}, \tag{1}$$

where $\sigma_{\rm exp(th)}$ is the fivefold experimental (or theoretical) differential cross section $(d^5\sigma/d\omega d\Omega_e d\Omega_p)$, (E_f, p_f) are the final proton energy and momentum, respectively, $f_{\rm rec}$ is a recoil factor [13] obtained by integrating over the binding energy of the bound state in the sixfold differential cross section, and $\sigma_{\rm cc1}$ is the de Forest [20] electron-proton off-shell cross section calculated using the FF parametrization of Ref. [18]. Within the PWIA, $\sigma_{\rm red}$ corresponds to the PWIA cross section from the scattering of a proton in the deuteron.

Figure 1 shows the extracted experimental and theoretical reduced cross sections as a function of p_r for three recoil angle settings at $Q^2 = 4.5 \pm 0.5$ $(\mathrm{GeV}/c)^2$. For the two highest momentum settings ($p_r = 580, 750$ MeV/c), a weighted average of the reduced cross sections were taken in the overlapping regions of p_r. The results from the previous experiment [11] at a $Q^2 = 3.5 \pm 0.25$ $(\mathrm{GeV}/c)^2$ are plotted as well (red square). The data are compared to theoretical calculations using wave functions determined from the charge-dependent Bonn (CD-Bonn) [21], Argonne v_{18} (AV18) [22], Paris [23], and WJC2 [24] NN potentials. The theoretical calculations for the CD-Bonn (magenta) and AV18 (green) potentials were performed by Sargsian [25] within the GEA, referred to as MS, and those for the Paris potential (blue) were by Laget [19] within the diagrammatic approach, referred to as JML. For the WJC2 (orange) potential, the calculations were carried out by Ford *et al.* [26] using a Bethe-Salpeter-like formalism for two-body bound states, which will be labeled JVO. The calculations use different FF parametrizations, which can lead to a ∼5.8%–6.6% variation of the theoretical cross section.

The difference between the deuteron wave functions with CD-Bonn, Paris, AV18, and WJC2 potentials is how the NN potential is modeled based on the empirical NN scattering data. The CD-Bonn model is based on the one-boson-exchange potential (OBEP) approach, in which the nucleon-meson-meson couplings are constrained to describe the NN scattering phase shifts extracted from the data. The interaction potential represents the static limit of this potential. In contrast, the WJC2 is a OBEP derived within the Covariant Spectator Theory [27–30], which requires comparatively few parameters while still producing a high-precision fit to the NN scattering data. The Paris and AV18 are purely phenomenological potentials, where a Yukawa-type interaction is introduced and parameters are fitted to describe the same NN scattering phase shifts. The major difference between the CD-Bonn and Paris, AV18, and WJC2 potentials is that the former predicts a much softer repulsive interaction at short distance, which results in a smaller high-momentum component in the deuteron wave function in momentum space. The effects of these local approximations on the NN potential are shown in Fig. 2 of Ref. [21].

For all recoil angles shown in Fig. 1 at recoil momenta $p_r \leq 250$ MeV/c, the cross sections are well reproduced by all models when FSIs are included. The agreement at $p_r \leq 250$ MeV/c can be understood from the fact that this region corresponds to the long-range part of the NN potential, where the one-pion-exchange potential is well known and common to all modern potentials.

Beyond $p_r \sim 250$ MeV/c at $\theta_{nq} = 35°$ and 45° [Figs. 1(a) and 1(b)], the JML, MS AV18, and JVO models increasingly differ from the MS CD-Bonn calculation.

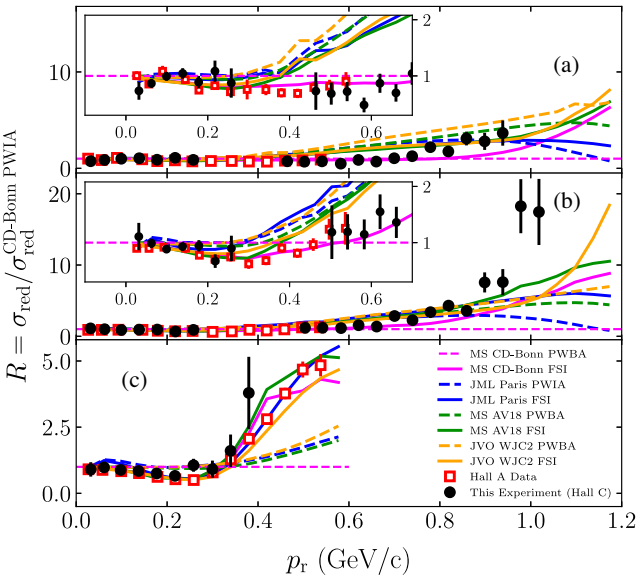

FIG. 2. The ratio $R(p_r)$ is shown in (a)–(c) for $\theta_{nq} = 35°$, 45°, and 75°, respectively, each with a bin width of ±5°. The dashed reference (magenta) line refers to MS CD-Bonn PWIA calculation (or momentum distribution) by which the data and all models are divided. Insets: enlargement of the subfigures for $p_r \leq 0.7$ GeV/c.

In this region, the JML and MS AV18 cross sections are dominated by the PWIA and in good agreement up to $p_r \sim 700$ MeV/c, whereas the JVO PWIA falls off with a comparatively smaller cross section at $\theta_{nq} = 35°$. The MS CD-Bonn cross sections in contrast are generally smaller than the JML, MS AV18 and JVO in this region. In addition, for $\theta_{nq} = 35°$, they are dominated by the PWIA up to $p_r \sim 800$ MeV/c [Fig. 1(a)], while for $\theta_{nq} = 45°$ FSIs start to contribute already above 600 MeV/c [Fig. 1(b)].

For recoil momenta $p_r \sim 0.55$–1.0 GeV/c [Figs. 1(a) and 1(b)], all models exhibit a steeper falloff compared to data. This discrepancy was quantified by doing a linear fit to the data and each of the PWIA calculations. A difference of at least 4.2 standard deviations was found between the data and theory slopes, which corresponds to a probability $\leq 1.1 \times 10^{-5}$ (very unlikely) that the observed discrepancy is due to a statistical fluctuation.

At $\theta_{nq} = 75°$ [Fig. 1(c)] and $p_r > 180$ MeV/c, FSIs become the dominant contribution to the cross sections for all models that exhibit a similar behavior (smaller falloff) that overshadows any possibility of extracting the approximate momentum distributions.

To quantify the discrepancy observed between data and theory in Fig. 1, the ratio of the experimental and theoretical reduced cross sections ($\sigma_{\rm red}$) to the deuteron momentum distribution calculated using the CD-Bonn potential ($\sigma_{\rm red}^{\rm CD\text{-}Bonn\ PWIA}$) [21] is shown in Fig. 2.

For $\theta_{nq} = 35°$ and 45° [Figs. 2(a) and 2(b)], the data are best described by the MS CD-Bonn PWIA calculation for recoil momenta up to $p_r \sim 700$ and ~600 MeV/c, respectively. Furthermore, the agreement between the Halls A and C data validates the Hall A approach of selecting a kinematic region where recoil angles are small and FSIs are reduced.

At larger recoil momenta, where the ratio $R > 1$ and increasing with p_r, for $\theta_{nq} = 35°$ FSIs start to dominate at $p_r \gtrsim 800$ MeV/c for the MS CD-Bonn calculation, while the other models predict still relatively small FSIs below 900 MeV/c. At $\theta_{nq} = 45°$, the FSI dominance starts earlier for all models above 800 MeV/c and for the MS CD-Bonn based calculation above 600 MeV/c.

Overall, it is interesting to note that none of the calculations can reproduce the measured p_r dependence above 600 MeV/c in a region where FSIs are still relatively small (< 30%). This behavior of the data is new and additional data in this kinematic region are necessary to improve the statistics.

At $\theta_{nq} = 75°$ [Fig. 2(c)], FSIs are small below $p_r \sim 180$ MeV/c, but do not exactly cancel the PWIA-FSI interference term in the scattering amplitude, which results in a small dip in this region in agreement with the data. At $p_r > 300$ MeV/c ($\theta_{nq} = 75°$), the data were statistically limited, as our focus was on the smaller recoil angles. The Hall A data, however, show a reasonable agreement with the FSIs from all models, which gives us confidence in our understanding of FSIs at the smaller recoil angles.

To summarize, this experiment extended the previous Hall A cross section measurements on the ^{2}H$(e, e'p)n$ reaction to $p_r > 500$ MeV/c at kinematics where FSIs were expected to be small and the cross sections were dominated by PWIA and sensitive to the short-range part of the deuteron wave function. The experimental reduced cross sections were extracted and found to be in good agreement with the Hall A data at lower recoil momenta where they overlap. Furthermore, the MS CD-Bonn model was found to be significantly different than the JML, MS AV18, or JVO models and was able to partially describe the data over a larger range in p_r. At the higher recoil momenta provided by this experiment ($p_r > 700$ MeV/c), however, all models were unable to describe the data, potentially illustrating the limit to which a nonrelativistic wave function from the solution to the Schrödinger equation is valid and able to describe experimental data that probe the high-momentum region of the np system in the most direct way possible. The new dataset is also ideal for testing fully relativistic deuteron models based on light-front [31] or covariant [32] formalisms. In this respect, the current effective-field-theories-based models [33] are nonrelativistic and might not have direct relevance to our data. Additional measurements of the ^{2}H$(e, e'p)n$ would be required to reduce the statistical uncertainties in this very high recoil momentum region ($p_r > 500$ MeV/c) to better understand the large deviations observed between the different models and data.

We acknowledge the outstanding support of the staff of the Accelerator and Physics Divisions at Jefferson Lab as well as the entire Hall C staff, making all four commissioning experiments possible. We would also like to thank Misak Sargsian, J. M. Laget, Sabine Jeschonnek, and J. W. Van Orden for providing the theoretical calculations, as well as the useful discussions we had on this topic. This work was supported in part by the U.S. Department of Energy (DOE), Office of Science, Office of Nuclear Physics under Award No. DE-SC0013620 and Contract No. DE-AC05-06OR23177, the Nuclear Regulatory Commission (NRC) Fellowship under Grant No. NRC-HQ-84-14-G-0040, the Doctoral Evidence Acquisition (DEA) Fellowship, and the Natural Sciences and Engineering Research Council of Canada (NSERC).

*cyero@jlab.org

[1] R. Subedi *et al.*, Probing cold dense nuclear matter, Science **320**, 1476 (2008).
[2] I. Korover *et al.* (Jefferson Lab Hall A Collaboration), Probing the Repulsive Core of the Nucleon-Nucleon Interaction via the $^4\mathrm{He}(e,e'pN)$ Triple-Coincidence Reaction, Phys. Rev. Lett. **113**, 022501 (2014).
[3] M. Duer *et al.* (CLAS Collaboration), Direct Observation of Proton-Neutron Short-Range Correlation Dominance in Heavy Nuclei, Phys. Rev. Lett. **122**, 172502 (2019).
[4] A. Schmidt, J. Pybus, R. Weiss *et al.*, Probing the core of the strong nuclear interaction, Nature (London) **578**, 540 (2020).
[5] E. Piasetzky, M. Sargsian, L. Frankfurt, M. Strikman, and J. W. Watson, Evidence for Strong Dominance of Proton-Neutron Correlations in Nuclei, Phys. Rev. Lett. **97**, 162504 (2006).
[6] F. Benmokhtar *et al.* (Jefferson Lab Hall A Collaboration), Measurement of the $^3\mathrm{He}(e,e'p)pn$ Reaction at High Missing Energies and Momenta, Phys. Rev. Lett. **94**, 082305 (2005).
[7] M. M. Rvachev *et al.* (Jefferson Lab Hall A Collaboration), Quasielastic $^3\mathrm{He}(e,e'p)^2\mathrm{H}$ Reaction at $Q^2 = 1.5$ GeV^2 for Recoil Momenta up to 1 GeV/c, Phys. Rev. Lett. **94**, 192302 (2005).
[8] W. Boeglin and M. Sargsian, Modern studies of the deuteron: From the lab frame to the light front, Int. J. Mod. Phys. E **24**, 1530003 (2015).
[9] M. M. Sargsian, Selected topics in high energy semi-exclusive electro-nuclear reactions, Int. J. Mod. Phys. E **10**, 405 (2001).
[10] L. L. Frankfurt, M. M. Sargsian, and M. I. Strikman, Feynman graphs and generalized eikonal approach to high energy knock-out processes, Phys. Rev. C **56**, 1124 (1997).
[11] W. U. Boeglin *et al.* (Hall A Collaboration), Probing the High Momentum Component of the Deuteron at High Q^2, Phys. Rev. Lett. **107**, 262501 (2011).
[12] K. S. Egiyan *et al.* (CLAS Collaboration), Experimental Study of Exclusive $^2\mathrm{H}(e,e'p)n$ Reaction Mechanisms at High Q^2, Phys. Rev. Lett. **98**, 262502 (2007).
[13] C. Yero, Cross section measurements of deuteron electrodisintegration at very high recoil momenta and large 4-momentum transfers (Q^2), Ph.D. thesis, Florida International University, Miami, Florida, 2020, https://arxiv.org/abs/2009.11343.
[14] R. Ent, B. W. Filippone, N. C. R. Makins, R. G. Milner, T. G. O'Neill, and D. A. Wasson, Radiative corrections for $(e,e'p)$ reactions at GeV energies, Phys. Rev. C **64**, 054610 (2001).
[15] See Supplemental Material at http://link.aps.org/supplemental/10.1103/PhysRevLett.125.262501 analysis details on the extraction of the cross sections, which include Refs. [16,17].
[16] R. Barlow, Systematic errors: Facts and fictions, arXiv:hep-ex/0207026.
[17] R. Barlow, Systematic Errors in Particle Physics (2017), https://indico.cern.ch/event/591374/contributions/2511753/attachments/1429002/2193943/01_PWA-Barlow.pdf.
[18] J. Arrington, Implications of the discrepancy between proton form factor measurements, Phys. Rev. C **69**, 022201(R) (2004).
[19] J. Laget, The electro-disintegration of few body systems revisited, Phys. Lett. B **609**, 49 (2005).
[20] T. de Forest, Off-shell electron-nucleon cross sections: The impulse approximation, Nucl. Phys. **A392**, 232 (1983).
[21] R. Machleidt, High-precision, charge-dependent Bonn nucleon-nucleon potential, Phys. Rev. C **63**, 024001 (2001).
[22] R. B. Wiringa, V. G. J. Stoks, and R. Schiavilla, Accurate nucleon-nucleon potential with charge-independence breaking, Phys. Rev. C **51**, 38 (1995).
[23] M. Lacombe, B. Loiseau, J. M. Richard, R. V. Mau, J. Côté, P. Pirès, and R. de Tourreil, Parametrization of the Paris $N-N$ potential, Phys. Rev. C **21**, 861 (1980).
[24] F. Gross and A. Stadler, High-precision covariant one-boson-exchange potentials for np scattering below 350 MeV, Phys. Lett. B **657**, 176 (2007).
[25] M. M. Sargsian, Large Q^2 electrodisintegration of the deuteron in the virtual nucleon approximation, Phys. Rev. C **82**, 014612 (2010).
[26] W. P. Ford, S. Jeschonnek, and J. W. Van Orden, Momentum distributions for $^2\mathrm{H}(e,e'p)$, Phys. Rev. C **90**, 064006 (2014).
[27] F. Gross, Three-dimensional covariant integral equations for low-energy systems, Phys. Rev. **186**, 1448 (1969).
[28] F. Gross, New theory of nuclear forces. relativistic origin of the repulsive core, Phys. Rev. D **10**, 223 (1974).
[29] F. Gross, Relativistic few-body problem. I. Two-body equations, Phys. Rev. C **26**, 2203 (1982).
[30] F. Gross, Relativistic few-body problem. II. Three-body equations and three-body forces, Phys. Rev. C **26**, 2226 (1982).
[31] L. Frankfurt and M. Strikman, High-energy phenomena, short range nuclear structure and QCD, Phys. Rep. **76**, 215 (1981).
[32] W. W. Buck and F. Gross, A family of relativistic deuteron wave functions, Phys. Rev. D **20**, 2361 (1979).
[33] P. Reinert, H. Krebs, and E. Epelbaum, Semilocal momentum-space regularized chiral two-nucleon potentials up to fifth order, Eur. Phys. J. A **54**, 86 (2018).